Principles Governing Conformations in Stereoisomeric Adducts of Bay Region Benzo[*a*]pyrene Diol Epoxides to Adenine in DNA: Steric and Hydrophobic Effects Are Dominant

Jian Tan, Nicholas E. Geacintov,*,† and Suse Broyde*,‡

Contribution from the Chemistry and Biology Departments, New York University, New York, New York 10003

Received October 8, 1999

Abstract: The stereochemical properties of ligands that form covalent adducts with DNA have profound effects on their biochemical functions. Differing absolute configurations of substituents about chiral carbon atoms can lead to strikingly different conformations when such stereoisomeric compounds bind to DNA. The environmental chemical carcinogen, benzo[*a*]pyrene (BP), provides a remarkable example of such stereochemical effects. Metabolic activation of benzo[*a*]pyrene leads to a pair of enantiomers, (+)-(7*R*,8*S*,9*S*,10*R*)-7,8-dihydroxy-9,10-epoxy-7,8,9,10-tetrahydrobenzo[*a*]pyrene and its (−)-(7*S*,8*R*,9*R*,10*S*) mirror-image, known as (+)- and (−)-*anti*-BPDE. Both (+)- and (−)-*anti*-BPDE react with the amino group of adenine in DNA via *trans* epoxide opening, yielding a pair of stereochemically distinct *trans-anti*-benzo[*a*]pyrenyl adducts, whose possible role in chemical carcinogenesis is of great interest. High-resolution NMR solution studies (Schurter et al. *Biochemistry* **1995**, *34*, 1364−75; Yeh et al. *Biochemistry* **1995**, *34*, 13570−81; Zegar et al. *Biochemistry* **1996**, *35*, 6212−24; Schwartz et al., *Biochemistry* **1997**, *36*, 11069−76) have revealed that in the 10*S* (+)- and 10*R* (−)-*trans-anti* adducts, the BP is classically intercalated, residing on the 3′-side of the modified adenine in the (+)-*trans-anti* adduct and on the 5′-side in the (−) stereoisomer. To elucidate the stereochemical principles underlying these conformational preferences, an extensive survey of the potential energy surface of each modified nucleoside was carried out, in which the energy of 373,248 structures for each adduct was computed using AMBER 5.0. Our results reveal near mirror image symmetries in the four pairs of low-energy structural domains of 10*S* (+)- and 10*R* (−)-*trans-anti*-[BP]−N^6-dA adducts, which is rooted in the exact enantiomeric relationship of the BPDE precursors, and accounts for the opposite orientations observed in solution. Steric hindrance prevents an *R* isomer from assuming the orientation favored by the *S* isomer, and vice versa. The NMR solution structures of 10*S* (+)- and 10*R* (−)-*trans-anti*-[BP]−N^6-dA adducts in DNA adopt conformations which are in the low-energy domains computed for the nucleoside adducts. In addition, we find that the preference for classical intercalation over a major groove position for the pyrenyl ring system in the [BP]−N^6-dA adducts stems from the advantage of burying the hydrophobic pyrenyl moiety within the helix rather than having it exposed in the large major groove.

Introduction

Polycyclic aromatic hydrocarbons (PAH) are products of fossil fuel combustion and are therefore ubiquitous as contaminants in the environment. Benzo[*a*]pyrene (BP) is a representative polycyclic aromatic hydrocarbon that is metabolically activated to potent oxygenated electrophiles which bind covalently to cellular DNA, thereby causing mutations which can induce cancer.[1,2] BP can be metabolically activated by the diol epoxide pathway,[3] as well as by one-electron oxidation,[4] and by the formation of reactive *o*-quinones.[5] The metabolic activation of BP via the predominant diol epoxide pathway leads to a number of products, including a pair of enantiomers, (+)-(7*R*,8*S*,9*S*,10*R*)-7,8-dihydroxy-9,10-epoxy-7,8,9,10-tetrahydrobenzo[*a*]pyrene and its (−)-(7*S*,8*R*,9*R*,10*S*) mirror-image, known as (+)- and (−)-*anti* BPDE[3] (Figure 1). While tumorigenicity is a complex multi-stage process,[2] it is interesting that in this case the (+)-enantiomer is highly tumorigenic in rodents while (−)-*anti*-BPDE is not.[6,7] Both enantiomers react with the amino groups of purines[8−10] in DNA via *cis* and *trans* epoxide opening, producing [BP]−N^2-dG and [BP]−N^6-dA adducts. The formation of these stable DNA adducts has been correlated with tumorigenesis in animal model systems.[11] While the guanine adducts are more predominant than the adenine adducts, the adenine adducts are mutagenic[12−15] in vitro and in vivo. The

* Corresponding authors. Telephone: (212) 998-8407. Fax: (212) 998-8421. E-mail: ng1@is.nyu.edu. Telephone: (212) 998-8231. Fax: (212) 995-4015. E-mail: broyde@nyu.edu.

† Chemistry Department.

‡ Biology Department.

(1) Garner, R. C. *Mutat. Res.* **1998**, *402*, 67−75.

(2) Weinberg, R. A. *Sci. Am.* **1996**, *275*, 62−70.

(3) Conney, A. H. *Cancer Res.* **1982**, *42*, 4875−917.

(4) Cavalieri, E. L.; Rogan, E. G. *Xenobiotics* **1995**, *25*, 677−688.

(5) Burczynski M. E.; Harvey R. G.; Penning T. M. *Biochemistry* **1998**, *37*, 6781−6790.

(6) Buening, M. K.; Wislocki, P. G.; Levin, W.; Yagi, H.; Thakker, D. R.; Akagi, H.; Koreeda, M.; Jerina, D. M.; Conney, A. H. *Proc. Natl. Acad. Sci. U.S.A.* **1978**, *75*, 5358−61.

(7) Slaga, T. J.; Bracken, W. J.; Gleason, G.; Levin, W.; Yagi, H.; Jerina, D. M.; Conney, A. H. *Cancer Res.* **1979**, *39*, 67−71.

(8) Cheng, S. C.; Hilton, B. D.; Roman, J. M.; Dipple, A. *Chem. Res. Toxicol.* **1989**, *2*, 334−40.

(9) Meehan, T.; Straub, K. *Nature* **1979**, *277*, 410−2.

(10) Brookes, P.; Osborne, M. R. *Carcinogenesis* **1982**, *3*, 1223−6.

(11) Ross, J. A.; Nelson, G. B.; Wilson, K. H.; Rabinowitz, J. R.; Galati, A.; Stoner, G. D.; Nesnow, S.; Mass, M. J. *Cancer Res.***1995**, *55*, 1039−1044.

10.1021/ja993624h CCC: $19.00
Published on Web 03/21/2000

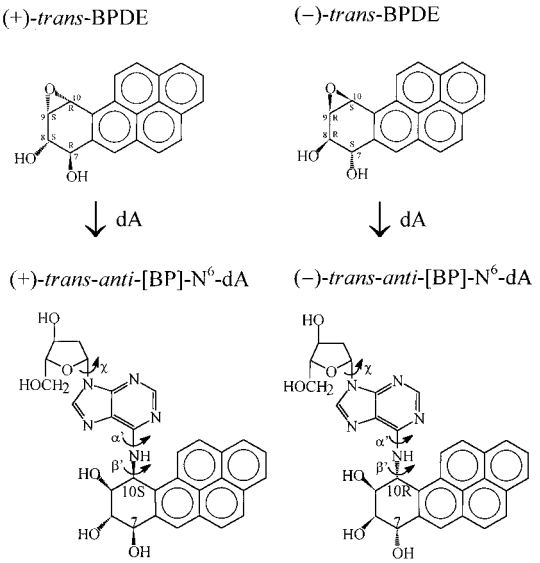

Figure 1. Structures of (+)- and (−)-*anti*-BPDE and (+)- and (−)-*trans-anti*-[BP]−N^6-dA nucleoside adducts. Torsion angles χ, α', β' are defined as follows: χ, O4′−C1′−N9−C4; α', N1−C6−N^6−C10(BP); β', C2−N^6−C10(BP)−C9(BP).

contribution of adenine adducts in general to chemical carcinogenesis may be very important,[16] and disproportionate relative to their abundance in cellular DNA because of higher excision efficiencies of the major guanine adducts by DNA repair proteins. For example, in some mammalian cells, *anti*-[BP]−N^6-dA adducts appear to be excised less efficiently from the transcribed DNA strand than *anti*-[BP]−N^2-dG adducts,[15] indicating they may indeed be more persistent in vivo than *anti*-[BP]−N^2-dG adducts.

One important reason for the different biological properties of adducts derived from the binding of *anti*-BPDE with guanine and adenine residues in DNA may be their conformations and thus their modes of interaction with DNA repair proteins and replicative enzymes. High-resolution NMR solution structures of guanine and adenine BPDE adducts embedded in various DNA sequences in solution have recently become available,[17−28] and are providing important new insights into the puzzling relationship between PAH carcinogen metabolite structure, stereochemistry, and adduct conformation.[29−31] The interplay between steric hindrance effects, base-base hydrogen bonding, and hydrophobic carcinogen-base stacking interactions, are the dominant effects that dictate the major types of PAH−DNA adduct conformations.[29] Three different conformational themes have been elucidated so far in normal, double-stranded DNA: positioning of the BP moiety (1) in the minor groove of B-DNA,[17−19] (2) in a base displaced-intercalated mode in which the carcinogen residue is intercalatively inserted between adjacent base pairs, displacing the modified base, guanine, and the partner cytidine from interior to exterior DNA sites,[20−24a] and (3) in a distorted classical intercalation position, in which the modified base, adenine, remains within the double helix and the covalently bound PAH residue is intercalated between the modified base pair and an adjacent pair.[24b,c−28] All of these structurally diverse conformations are assumed by BP residues when different *anti*-BPDE stereoisomers bind to guanine or adenine residues in DNA.

A fascinating generalization has emerged from these and other structures of adducts derived from mirror-image (+)- and (−)-*anti* diol epoxide enantiomers. Regardless of the base modified, the number of aromatic rings in the PAH residue, or the specific position of the aromatic moiety with respect to the DNA bases, adducts derived from a pair of (+)- and (−)-*anti* diol epoxide enantiomers are always aligned in opposite directions relative to the modified adenine or guanine base[17−28,32−38] in the DNA duplex. Thus, the guanine adducts, (+)- and (−)-*trans-anti*-[BP]−N^2-dG, are oriented 5′ or 3′ along the modified strand in the minor groove, respectively, in normal full duplexes.[17−19] In contrast, in the (+)- and (−)-*cis-anti*-[BP]−N^2-dG adducts, the BP moiety is inserted into the interior of the helix, and the modified guanine is displaced out of the helix; in the case of the (+)-*cis-anti* adduct, the pyrenyl aromatic residue is directed toward the *major* groove, while in the case of the (−)-*cis-anti*-

(12) Christner, D. F.; Lakshman, M. K.; Sayer, J. M.; Jerina, D. M.; Dipple, A. *Biochemistry* **1994**, *33*, 14297−305.
(13) Chary, P.; Latham, G. J.; Robberson, D. L.; Kim, S. J.; Han, S.; Harris, C. M.; Harris, T. M.; Lloyd, R. S. *J. Biol. Chem.* **1995**, *270*, 4990−5000.
(14) Page, J. E.; Zajc, B.; Oh-hara, T.; Lakshman, M. K.; Sayer, J. M.; Jerina, D. M.; Dipple, A. *Biochemistry* **1998**, *37*, 9127−37.
(15) Wei, S. J.; Chang, R. L.; Bhachech, N.; Cui, X. X.; Merkler, K. A.; Wong, C. Q.; Hennig, E.; Yagi, H.; Jerina, D. M.; Conney, A. H. *Cancer Res.* **1993**, *53*, 3294−301.
(16) Dipple, A.; Pigott, M. A.; Agarwal, S. K.; Yagi, H.; Sayer, J. M.; Jerina, D. M. *Nature* **1989**, *327*, 535−536.
(17) Cosman, M.; de los Santos, C.; Fiala, R.; Hingerty, B. E.; Singh, S. B.; Ibanez, V.; Margulis, L. A.; Live, D.; Geacintov, N. E.; Broyde, S. *Proc. Natl. Acad. Sci. U.S.A.* **1992**, *89*, 1914−8.
(18) Fountain, M. A.; Krugh, T. R. *Biochemistry* **1995**, *34*, 3152−61.
(19) de los Santos, C.; Cosman, M.; Hingerty, B. E.; Ibanez, V.; Margulis, L. A.; Geacintov, N. E.; Broyde, S.; Patel, D. J. *Biochemistry* **1992**, *31*, 5245−52.
(20) Cosman, M.; Fiala, R.; Hingerty, B. E.; Amin, S.; Geacintov, N. E.; Broyde, S.; Patel, D. J. *Biochemistry* **1994**, *33*, 11518−27.
(21) Cosman, M.; Fiala, R.; Hingerty, B. E.; Amin, S.; Geacintov, N. E.; Broyde, S.; Patel, D. J. *Biochemistry* **1994**, *33*, 11507−17.
(22) Cosman, M.; de los Santos, C.; Fiala, R.; Hingerty, B. E.; Ibanez, V.; Luna, E.; Harvey, R.; Geacintov, N. E.; Broyde, S.; Patel, D. J. *Biochemistry* **1993**, *32*, 4145−55.
(23) Cosman, M.; Hingerty, B. E.; Luneva, N.; Amin, S.; Geacintov, N. E.; Broyde, S.; Patel, D. J. *Biochemistry* **1996**, *35*, 9850−63.
(24) (a) Feng, B.; Gorin, A.; Kolbanovskiy, A.; Hingerty, B. E.; Geacintov, N. E.; Broyde, S.; Patel, D. J. *Biochemistry* **1997**, *36*, 13780−90. (b) Schurter, E. J.; Sayer, J. M.; Oh-hara, T.; Yeh, H. J. C.; Yagi, H.; Luxon, B. A.; Jerina, D. M.; Gorenstein, D. G. *Biochemistry* **1995**, *34*, 9009−9020. (c) Mao, B.; Gu, Z.; Gorin, A.; Chen, J.; Hingerty, B. E.; Amin, S.; Broyde, S.; Geacintov, N. E.; Patel, D. J. *Biochemistry* **1999**, *38*, 10831−10842.
(25) Yeh, H. J.; Sayer, J. M.; Liu, X.; Altieri, A. S.; Byrd, R. A.; Lakshman, M. K.; Yagi, H.; Schurter, E. J.; Gorenstein, D. G.; Jerina, D. M. *Biochemistry* **1995**, *34*, 13570−81.
(26) Schwartz, J. L.; Rice, J. S.; Luxon, B. A.; Sayer, J. M.; Xie, G.; Yeh, H. J.; Liu, X.; Jerina, D. M.; Gorenstein, D. G. *Biochemistry* **1997**, *36*, 11069−76.
(27) Zegar, I. S.; Kim, S. J.; Johansen, T. N.; Horton, P. J.; Harris, C. M.; Harris, T. M.; Stone, M. P. *Biochemistry* **1996**, *35*, 6212−24.
(28) Schurter, E. J.; Yeh, H. J.; Sayer, J. M.; Lakshman, M. K.; Yagi, H.; Jerina, D. M.; Gorenstein, D. G. *Biochemistry* **1995**, *34*, 1364−75.
(29) Geacintov, N. E.; Cosman, M.; Hingerty, B. E.; Amin, S.; Broyde, S.; Patel, D. J. *Chem. Res. Toxicol.* **1997**, *10*, 111−46.
(30) Xie, X. M.; Geacintov, N. E.; Broyde, S. *Biochemistry* **1999**, *38*, 2956−68.
(31) Xie, X. M.; Geacintov, N. E.; Broyde, S. *Chem. Res. Toxicol.* **1999**, *12*, 597−609.
(32) Singh, S. B.; Hingerty, B. E.; Singh, U. C.; Greenberg, J. P.; Geacintov, N. E.; Broyde, S. *Cancer Res.* **1991**, *51*, 3482−92.
(33) Jerina, D. M.; Sayer, J. M.; Yeh, H. J. C.; Liu, X.; Yagi, H.; Schurter, E.; Gorenstein, D. *Polycyclic Aromat. Hydrocarbons* **1997**, *10*, 145−152.
(34) Cosman, M.; Laryea, A.; Fiala, R.; Hingerty, B. E.; Amin, S.; Geacintov, N. E.; Broyde, S.; Patel, D. J. *Biochemistry* **1995**, *34*, 1295−307.
(35) Cosman, M.; Fiala, R.; Hingerty, B. E.; Laryea, A.; Lee, H.; Harvey, R. G.; Amin, S.; Geacintov, N. E.; Broyde, S.; Patel, D. *Biochemistry* **1993**, *32*, 12488−97.
(36) Zegar, I. S.; Setayesh, F. R.; DeCorte, B. L.; Harris, C. M.; Harris, T. M.; Stone, M. P. *Biochemistry* **1996**, *35*, 4334−48.
(37) Feng, B.; Voehler, M.; Zhou, L.; Passarelli, M.; Harris, C. M.; Harris, T. M.; Stone, M. P. *Biochemistry* **1996**, *35*, 7316−29.
(38) Feng, B.; Zhou, L.; Passarelli, M.; Harris, C. M.; Harris, T. M.; Stone, M. P. *Biochemistry* **1995**, *34*, 14021−36.

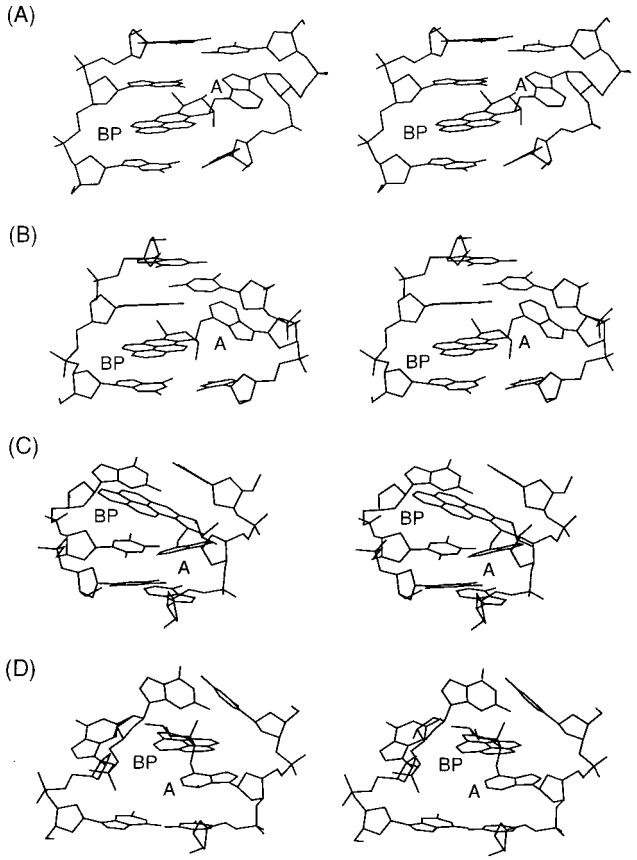

Figure 2. NMR solution structures of (+)- and (−)-*trans-anti*-[BP]−N^6-dA adducts. (A) (+)-*trans* A−G mismatch major conformer.[25] (B) (+)-*trans* A−G mismatch minor conformer.[26] (C) (−)-*trans* A−T normal partner.[27] (D) (−)-*trans* A−G mismatch conformer.[28] Central modified duplex 5-mer is shown in stereo.

[BP]−N^2-dG adduct, it is directed toward the *minor* groove.[20,22,23] Opposite orientations are also observed in the case of the adenine adducts. In the (+)-*trans-anti*-[BP]−N^6-dA adduct with 10*S* stereochemistry at the linkage site, the intercalated BP residue is inserted on the 3′-side of the modified, nondisplaced adenine, while in the case of the 10*R* (−)-*trans-anti* adduct it is inserted on the 5′-side of the modified adenine residue.[25−28]

It is of fundamental interest to elucidate the origin of the opposite orientations in 10*S* and 10*R* adducts. Our preliminary studies had suggested that steric hindrance involving atoms on the BP and covalently linked purine residues are essentially at the root of the opposite orientation phenomenon;[29] this is termed "primary" steric hindrance. In contrast, steric close contacts with neighboring atoms on other DNA residues are called secondary steric hindrance effects.[29] Thorough surveys of the potential energy surfaces of the stereoisomeric [BP]−N^2-dG mononucleoside adduct level have been previously performed to investigate the energetically preferred conformations of the 10*S* (+)- and 10*R* (−)-*trans-anti*−N^2-dG adducts, and the 10*R* (+)- and 10*S* (−)-*cis-anti*-[BP]−N^2-dG adducts.[30,31] These studies elucidated the fundamental origins governing the conformations adopted by these stereoisomeric adducts in DNA duplexes. The energetically favored conformational domains computed at the nucleoside level are observed in the high-resolution NMR solution structures of the DNA duplexes.[17−24a]

In the present work, we focus on the origins of the intercalative conformations and opposite orientations of the adducts derived from the binding of (+)- and (−)-*anti*-BPDE to N^6 of deoxyadenosine in DNA, by examining the 10*S* (+)- and 10*R* (−)-*trans-anti*-[BP]−N^6-dA adducts at the mononucleoside level. Figure 1 shows structures of the 10*S* (+)- and 10*R* (−)-*trans-anti*-[BP]−N^6-dA adducts.

Our goal is to determine the stereochemical and physical-chemical factors that govern the classical intercalation-type conformations, with opposite orientations relative to the modified deoxyadenosine residues, of the 10*S* (+)- and 10*R* (−)-*trans-anti*-[BP]−N^6-dA adducts. Of particular interest is the striking difference between the classically intercalated [BP]−N^6-dA adduct conformations and the minor groove or base-displaced intercalative conformations of the 10*S* (+)- and 10*R* (−)-*trans-anti*-[BP]−N^2-dG adducts with the same absolute configurations at C10. To accomplish these goals, an extensive survey of the potential energy surface was made for the (+)- and (−)-*trans-anti*-[BP]−N^6-dA mononucleoside adducts using AMBER 5.0 with the recent Cornell et al. force field.[39]

Our results reveal near mirror image symmetries in the four pairs of low-energy structures of 10*S* (+)- and 10*R* (−)-*trans-anti*-[BP]−N^6-dA adducts, which account for the opposite orientations observed in the high-resolution NMR structures, shown in Figure 2. Overall, the observed solution NMR structures of 10*S* (+)- and 10*R* (−)-*trans-anti*-[BP]−N^6-dA adducts in double stranded DNA are in low-energy domains computed here for the mononucleoside adducts.[25−28] (See Discussion for details concerning the single exception.[28]) In addition, we elucidate that the preference for classical intercalation over a major groove position for the pyrenyl ring system in the [BP]−N^6-dA adducts stems from the advantage of burying the hydrophobic pyrenyl moiety within the helix rather than having it exposed on both faces in the large major groove.

Methods

Creating Starting Conformations. Coordinates of high-resolution NMR solution structures of the (+)- and (−)-*trans-anti*-[BP]−N^6-dA adducts in 9-mer double stranded DNA sequences,[25,28] kindly provided by Dr. Jane M. Sayer, were employed. The modified base was excised from the duplex 9-mer containing the major conformer of the (+)-*trans-anti*-[BP]−N^6-dA adduct mismatched with dG.[25] The same procedure was employed for the (−)-*trans-anti* adduct.[28] These were minimized with AMBER 5.0, as described below in the Energy Computation section. The energy minimized structures contained benzylic ring conformations in the same family (distorted half chair, H9, H10 pseudoequatorial, H7, H8 pseudoaxial, defined by internal dihedral angles given in Supporting Information, Table S1) as the starting structures, but they became essentially exact mirror images following minimization (Supporting Information, Table S1). This provided the geometry for the base and BP moiety in our study. The geometry of the sugar was obtained in a separate step: the modified nucleoside was excised from the (+)-*trans-anti* adduct, with hydrogens substituted for the O3′ and O5′ phosphorus atoms, and its energy minimized. The resultant sugar geometry was utilized for both adducts: sugar pseudorotation parameter[40] P = 28.38°; C3′−C4′−C5′−O5′ torsion $\gamma = -179.66°$; C4′−C5′−O5′−H5′ torsion $\beta = -47.11°$; C4′−C3′−O3′−H3′ torsion $\epsilon = -77.58°$. The program INSIGHTII from MSI, Inc. was employed for computer graphic manipulations and to render structures for visualization.

Starting structures for the energy calculations were then created with a torsion driver, a program which rotates the torsion angles χ, α', β' (Figure 1) to selected values and then computes the coordinates of the resulting structures. The starting structures uniformly surveyed the potential energy surface of the molecule with conformers in which χ, α', β' sampled their 360° conformation space at 5° intervals, in combination, giving a total of $(360°/5° = 72)^3 = 373{,}248$ conformers for each adduct.

(39) Cornell, W.; Cieplak, P.; Bayly, C. I.; Gould, I. R.; Merz, K. M.; Ferguson, D. M.; Spellmeyer, D. C.; Fox, T.; Caldwell, J. W.; Kollman, P. A. *J. Am. Chem. Soc.* **1995**, *117*, 5179−5197.

(40) Altona, A.; Sundaralingam, M. *J. Am. Chem. Soc.* **1972**, *94*, 8205−8212.

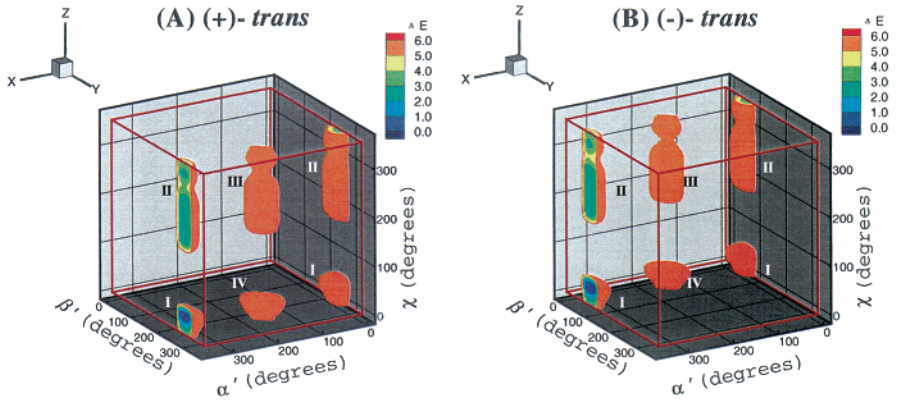

Figure 3. Three-dimensional χ, α' and β' energy topographies to 6 kcal/mol. I−IV denote the four low-energy domains. Torsion angles cycle over 360°, and thus 359° is actually contiguous with 0°: (A) (+)-*trans-anti*-[BP]−N^6-dA adduct; (B) (−)-*trans-anti*-[BP]−N^6-dA adduct.

Energy Computation. Energies of each of the 373,248 structures for each adduct were computed with the molecular mechanics program AMBER 5.0,[41] using the Cornell et al. force field[39] with the PARM96.DAT parameter set. Since there are no negatively charged phosphates in the nucleoside, Na^+ counterions were not needed. A sigmoidal distance dependent dielectric function,[42] a reasonable treatment for the dielectric constant,[43] was employed in the Coulombic term of the force field to model the dielectric effects of solvent water. Parameters added to the AMBER 5.0 force field for the [BP]−N^6-dA adducts are given in Table S2. Partial charges for modified bases and nucleosides were computed with Gaussian 94[44] at basis set level 6-31G*, compatible with the rest of the AMBER 5.0 force field, and then the least squares charge fitting algorithm RESP[45] provided with AMBER 5.0 was used to fit the charge to each atomic center. Partial charges, atom types and topology information are given in Table S3, Supporting Information.

Where energy minimizations were carried out, we employed 100 cycles of steepest descent for the small BP-modified base or nucleoside, and 1000 cycles for the 11-mer duplex major groove conformer (see below in Methods section: Modeling a Major Groove Conformer in a DNA Duplex), followed by conjugate gradient minimization to convergence, using a convergence criterion of 10^{-4} kcal/mol Å.

Statistical Weights and Thermodynamic Quantities. The computed AMBER energies for each of the 373,248 structures created for each adduct were used to construct both three-dimensional energy surfaces as a function of the χ, α', and β' torsion angles and two-dimensional energy contour slices through them; slices were made at 5° intervals of χ as a function of α', β', and also at selected β' values as a function of χ, α'. The program TECPLOT was used for this purpose. These plots revealed four low-energy wells or domains (Figure 3). This permitted grouping the full data set into four regions, each of which encompassed one of the four low-energy domains:

Region 1:
$\chi = 0°-125°$; $\alpha' = 270°-355°$ and $0°-85°$; $\beta' = 0°-355°$

Region 2:
$\chi = 130°-355°$; $\alpha' = 270°-355°$ and $0°-85°$; $\beta' = 0°-355°$

Region 3: $\chi = 130°-355°$; $\alpha' = 90°-265°$; $\beta' = 0°-355°$

Region 4: $\chi = 0°-125°$; $\alpha' = 90°-265°$; $\beta' = 0°-355°$

With this grouping, we computed conformational free energies, enthalpies, entropies, and fractional statistical weights for each low-energy domain, using standard thermodynamic relationships.[46]

The fractional statistical weight, P_i, of each conformer was computed from the relationship

$$P_i = \frac{e^{-\Delta E_i/RT}}{\sum_{i=1}^{N} e^{-\Delta E_i/RT}}$$

where ΔE_i is the relative energy of a given conformer in kcal/mol with respect to the lowest-energy structure, R is the universal gas constant, 1.987×10^{-3} kcal/mol-deg, $T = 300°$ K, and N is 373,248, the total number of conformers for each adduct.

Using the above grouping, we computed the combined fractional statistical weight, W_j, for each region (containing one low-energy well) by summing the individual statistical weights, P_i, of each point in the region:

$$W_j = \sum_{i=1}^{n_i} P_i$$

where n_j is the number of conformers in each one of the four regions ($j = 1, 2, 3, 4$). In practice, only conformers with energies ΔE_i below 3 kcal/mol contribute significantly to the statistical weight of a given region, but all conformers in the region were included in the calculation.

The conformational free energy of each well, G_j, was then computed from the relationship

$$G_j = -RT \ln \sum_{i=1}^{n_j} e^{-\Delta E_i/RT}$$

To obtain the conformational entropy of each well, S_j, we first compute p_i, the fractional statistical weight of each conformer within its own well or region:

(41) Case, D.; Pearlman, D.; Caldwell, J.; Cheatham, T.; Ross, W.; Simmerling, C.; Darden, T.; Merz, K.; Stanton, R.; Cheng, A.; Vincent, J.; Crowley, M.; Ferguson, D.; Radner, R.; Seibel, G.; Singh, U. C.; Weiner, P.; Kollman, P. *AMBER 5.0*; University of California, 1997.

(42) Hingerty, B. E.; Ritchie, R. H.; Ferrell, T. L.; Turner, J. E. *Biopolymers* **1985**, *24*, 427−439.

(43) Friedman, R. A.; Honig, B. *Biopolymers* **1992**, *32*, 145−59.

(44) Frisch, M. J.; Trucks, G. W.; Schlegel, H. B.; Gill, P.; Johnsone, B. G.; Robb, M. A.; Cheeseman, J. R.; Keith, T. A.; Petersson, G. A.; Montgomery, J. A.; Raghavachari, K.; Al-Laham, M. A.; Zakrzewski, V. G.; Ortiz, J. V.; Foresman, J. B.; Cioslowski, J.; Stefanov, B. B.; Nanayakkara, A.; Challacombe, M.; Peng, C. Y.; Ayala, P. Y.; Chen, W.; Wong, M. W.; Andres, J. L.; Reploge, E. S.; Gomperts, R.; Martin, R. L.; Fox, D. J.; Binkley, J. S.; Defrees, D. J.; Baker, J.; Stewart, J. P.; Head-Gordon, M.; Gonzalez, C.; Pople, J. A. *Gaussian 94*, revision A.1; Gaussian: Pittsburgh, PA 1995.

(45) Bayly, C. I.; Cieplak, P.; Cornell, W. D.; Kollman, P. A. *J. Phys. Chem.* **1993**, *97*, 10269−80.

(46) Atkins, P. W. *Physical Chemistry*, 4th ed.; W. H. Freeman Co.: NY, 1990.

(47) Connolly, M. L. *Science* **1983** *221*, 709−713.

(48) Sharp, K. A.; Nicholls, A.; Fine, R. F.; Honig, B. *Science* **1991**, *252*, 106−9.

$$p_i = \frac{e^{-\Delta E_i/RT}}{\sum_{i=1}^{n_j} e^{-\Delta E_i/RT}}$$

Then,

$$S_j = -R\sum_{i=1}^{n_j} p_i \ln p_i$$

Conformational enthalpies for each well, H_j, are obtained from

$$G_j = H_j - TS_j$$

Hydrophobic Effect. The free energy cost of the entropic hydrophobic effect, $\Delta G_{\text{hydrophobic}}$, stemming from retaining aromatic rings in aqueous solvent was estimated by determining the solvent accessible surface area, ΔA, with the Connolly algorithm[47] in INSIGHTII, using a probe radius of 1.4 Å and INSIGHT default van der Waals radii. Only the aromatic atoms, without the hydrophilic benzylic ring, were included in the surface calculation. We used the relationship $\Delta G_{\text{hydrophobic}} = \gamma \Delta A$, where γ is an empirical parameter, 47 cal mol^{-1} Å^{-2} [48] to compute $\Delta G_{\text{hydrophobic}}$. This term was computed for modified DNA duplexes, but not for the modified nucleosides where solvent exposure of the BP moiety is essentially constant in all of the low-energy structures, and hence can be neglected.

Modeling a Major Groove Conformer in a DNA Duplex. We obtained an energy-minimized major groove conformer for the (+)-*trans-anti*-[BP]−N^6-dA adduct by starting with the analogous (*S*)-α isomer of the one-ring styrene oxide adduct,[37] which resides in the major groove. We replaced the styrene oxide adduct with the BP adduct in the 11-mer duplex sequence, manipulated the χ, α', β' values to minimize steric collisions, and minimized the energy with the same force field parameters used for the nucleoside adduct. Starting values for χ, α', β' were 215°, 180°, 0°.

Computations were carried out at the Department of Energy National Energy Research Supercomputer Center (Berkeley), the National Science Foundation National Partnership for Advanced Computational Infrastructure (San Diego) and on our own SGI workstations.

Results

Four Low-Energy Conformational Domains: Near Mirror Image Symmetry of Adducts Derived from (+)- and (−)-*anti*-BPDE Enantiomers. Figure 3 depicts the 3-dimensional AMBER energy topographies as a function of the torsion angles χ, α', and β', up to 6 kcal/mol above the lowest energy, for the 10*S* (+)- and 10*R* (−)-*trans-anti*-[BP]−N^6-dA adducts. We note that there are four low-energy domains (potential energy wells) for each of the two adducts. Domains I and IV have *syn* glycosidic torsion angles χ, and Domains II and III are in the *anti* region. Table 1 summarizes the ranges in the values of χ, α' and β' that characterize each of the four low-energy domains. Table 2 gives the number of conformers in each 1 kcal/mol energy shell from 0 to 5 kcal/mol. Tables S1 and S2 (Supporting Information) give the full set of α', β' energy contour maps at 5° intervals of χ, for the 10S(+)- and 10R(−)-*trans-anti*-[BP]−N^6-dA adducts, respectively.

Table 1. Domains of Low-Energy Wells in 10*S* (+)- and 10*R* (−)-*trans-anti*-[BP]−N^6-dA Adducts[a]

domain	χ domain (deg)	α' domain (deg)	β' domain(deg) (+) adduct	β' domain(deg) (−) adduct
I	35 + 25/ −35	0 ± 35	−90 ± 40	90 ± 40
II	215 + 145/ −35	0 ± 35	−90 ± 40	90 ± 40
III	215 + 145/ −35	180 ± 35	−90 ± 40	90 ± 40
IV	35 + 25/ −35	180 ± 35	−90 ± 40	90 ± 40

[a] Domains of the 6 kcal/mol surface were approximated to ±5°, from the approximate well center. χ and α' domains are the same for (+) and (−) adducts. For α' this is the case because 0° and 180° are the same as their sign inverted values.

To examine in more detail the relationship between the energy landscapes of the 10*S* (+)- and 10*R* (−)-*trans-anti* adducts as a function of the critical torsion angles α' and β' that govern the relative orientations of the BP and nucleoside residues (Figure 1), we generated slices through the approximate centers of the wells in the *syn* (35°) and *anti* (215°) domains of χ, to obtain energy contour maps in the α', β' plane (Figure 4). These 2-dimensional 10*S* (+)- and 10*R* (−)-*trans-anti* adduct maps clearly reveal a remarkable symmetry. The map for the (+) adduct can be essentially transformed into that of the (−) adduct by inverting the sign of the torsion angles α' and β'. This corresponds to a 180° rotation about a central symmetry axis positioned perpendicular to the map plane at α', $\beta' = 180°$, 180°. Thus, a given energy feature in a specific α', β' region of the (+) adduct map, has a corresponding feature in the (−) adduct map in the $-\alpha'$, $-\beta'$ region. Such torsion angle symmetry is a classical hallmark of mirror image pairs of molecules. However, the symmetry is not exact in our nucleoside adduct pair.

Transitions between Different Domains. The question arises whether the different conformational domains are connected to one another by relatively low-energy pathways. Examining the α', β' maps in Figure 4, it is evident that *anti* domains II and III are connected to one another at energies of about 20−22 kcal/mol, and the *syn* domains I and IV are connected by a 17−20 kcal/mol pathway. It is evident from the 3-dimensional χ, α', β' energy topography of Figure 3 that a path also exists between *syn* domain I and *anti* domain II along the $\chi = 0°$ trajectory. To elucidate this connectivity further, a two-dimensional energy contour slice was generated through the approximate centers of domains I and II, at $\beta' = 280°$ (−80°) for the (+)-*trans* adduct, and 80° for the (−)-*trans-anti* adduct. This map, shown in Figure S3 (Supporting Information), reveals the connecting path at about 5−6 kcal/mol. Similarly, Figure 3 also reveals a path between *syn* domain IV and *anti* domain III at $\chi = 0°$ at about 6−7 kcal/mol (Figure S3). These paths represent upper limits in the energy pathways, since our computations could only survey the key sources of conformational flexibility, the torsion angles χ, α', β'.

Low-Energy Conformations. Figure 5 shows color views of representative structures of each of the four low-energy

Table 2. Number of Conformations in 1 kcal/mol Shells in 10*S* (+)- and 10*R* (−)-*trans-anti*-[BP]−N^6-dA Adducts, to 5 kcal/mol

	0−1 kcal/mol		1−2 kcal/mol		2−3 kcal/mol		3−4 kcal/mol		4−5 kcal/mol		total	
domain	(+)	(−)	(+)	(−)	(+)	(−)	(+)	(−)	(+)	(−)	(+)	(−)
I	133	134	187	189	252	255	314	319	317	306	1203	1203
II	0	0	31	3	790	751	1055	973	1046	1080	2922	2808
III	0	0	0	0	0	0	113	103	412	400	525	503
IV	0	0	12	12	68	77	124	123	159	163	363	375
total	133	134	230	204	1110	1080	1606	1518	1934	1949	5013	4889

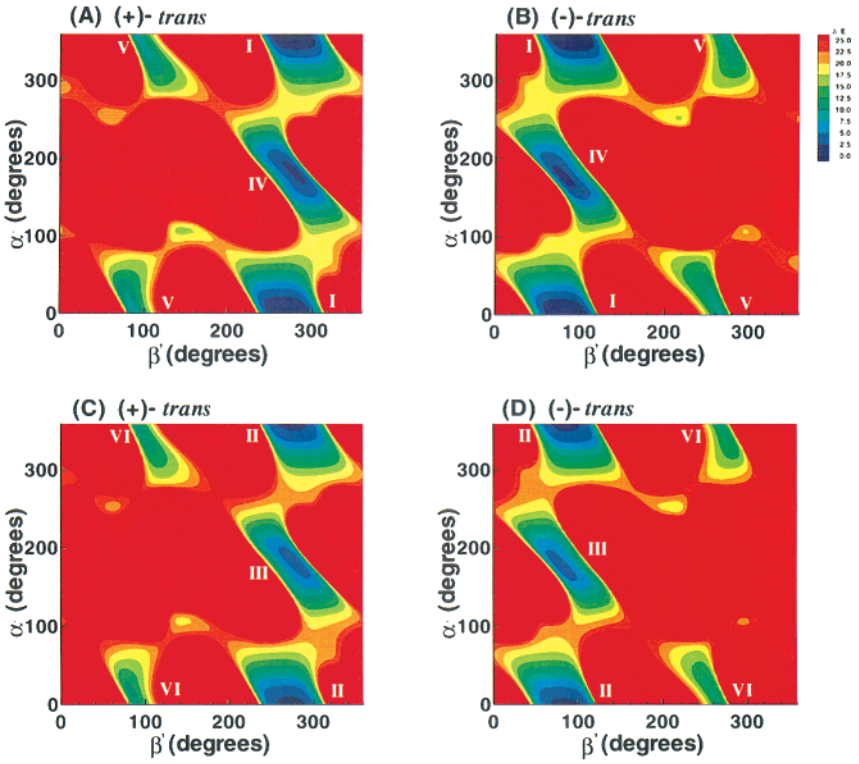

Figure 4. α', β' energy contour maps to 25 kcal/mol. I−IV denote the four low-energy domains. V and VI are higher-energy domains that do not contribute to the statistical weights. Torsion angles cycle over 360°, and thus 359° is actually contiguous with 0°: (A) (+)-*trans-anti*-[BP]−N^6-dA adduct, χ = 35°(*syn*); (B) (−)-*trans-anti*-[BP]−N^6-dA adduct, χ = 35°(*syn*); (C) (+)-*trans-anti*-[BP]−N^6-dA adduct, χ = 215°(*anti*); (D) (−)-*trans-anti*-[BP]−N^6-dA adduct, χ = 215°(*anti*).

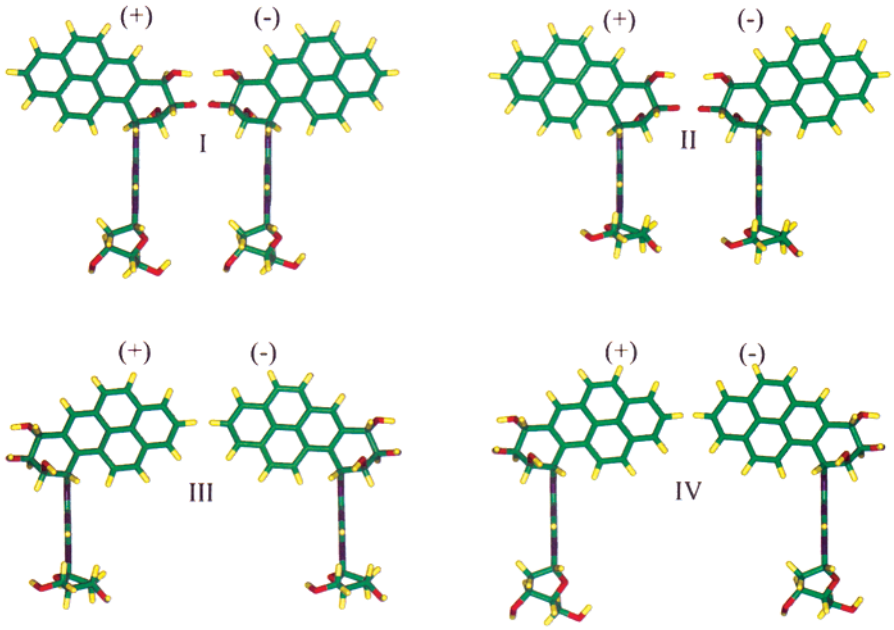

Figure 5. Color views of representative structures for (+)- and (−)-*trans-anti*-[BP]−N^6-dA adducts. I−IV denote the four low-energy domains. In each pair the left structure is the (+)-*trans-anti*-[BP]−N^6-dA adduct and the right is the (−) adduct. χ, α', and β' values and energies, ΔE, relative to the global minimum are the following. Domain I: (+) adduct 35°, 0°, 280°; (−) adduct 35°, 0°, 80°; ΔE (+) 0.00, (−) 0.01 kcal/mol. Domain II: (+) adduct 215°, 0°, 280°; (−) adduct 215°, 0°, 80°; ΔE (+) 3.66, (−) 3.71 kcal/mol. Domain III: (+) adduct 215°, 180°, 280°; (−) adduct 215°, 180°, 80°; ΔE (+) 1.93, (−) 2.00 kcal/mol. Domain IV: (+) adduct 35°, 180°, 280°; (−) adduct 35°, 180°, 80°; ΔE (+) 1.79, (−) 1.76 kcal/mol. The view is edge-on along the adenine with C8H directed toward the viewer.

domains of the (+) and (−) adducts. Figures 6 and 7 show these structures in stereo. Figure 5 shows that for each domain, the (+)-*trans-anti* adduct structure is nearly a mirror image of the (−)-*trans-anti* structure, with the mirror image symmetry broken only by the sugar residues. The nonchiral orientations of the sugar residues can be discerned by noting that the sugar O4′

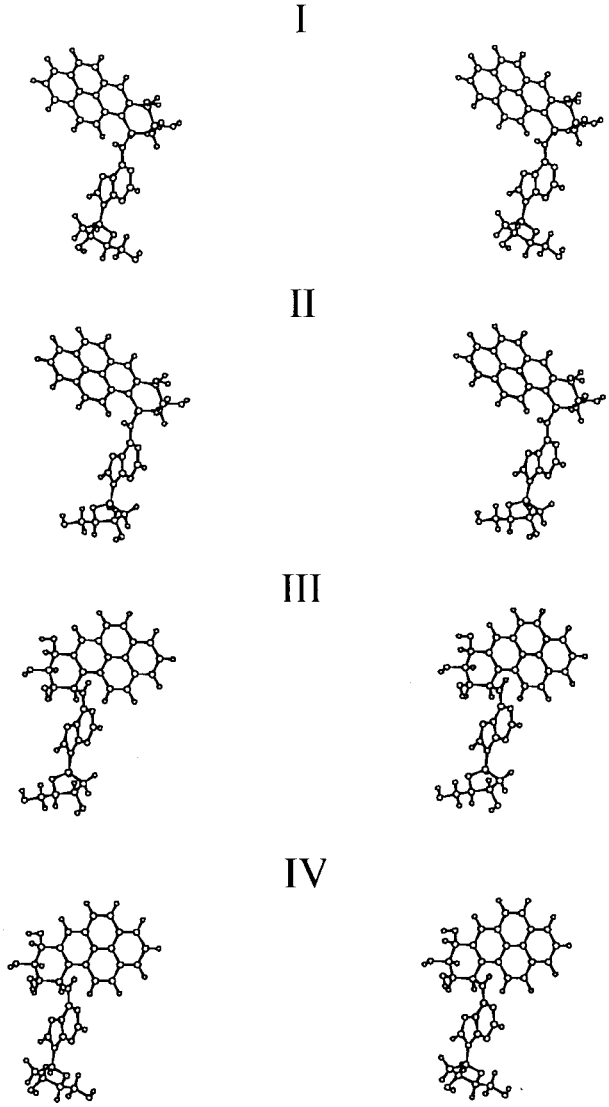

Figure 6. Stereoviews for (+)-*trans-anti*-[BP]−N^6-dA adduct. Representative structures of Figure 5. I−IV denote four low-energy domains.

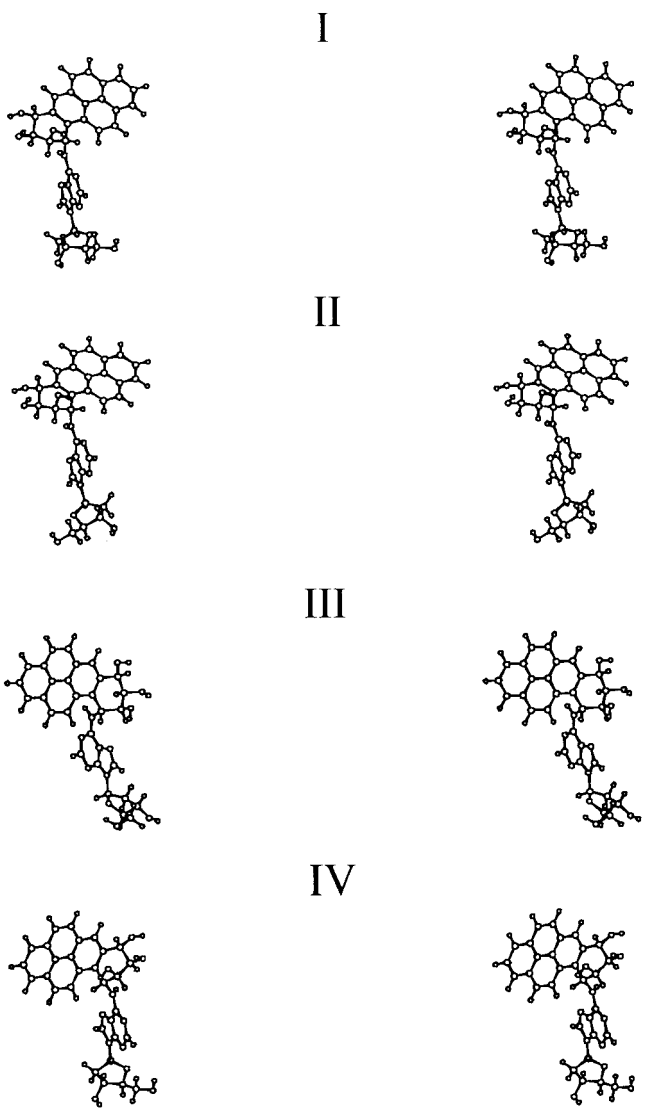

Figure 7. Stereoviews for (−)-*trans-anti*-[BP]−N^6-dA adduct. Representative structures of Figure 5. I−IV denote four low-energy domains.

atoms point in the same rather than the opposite directions in the case of the (+)- and (−)-*trans-anti* adducts in each domain.

The four structural types are approximately related to one another by torsional rotations as follows:

$$\text{Domain I} \xrightarrow{\chi + \sim 180^\circ} \text{Domain II}$$

$$\text{Domain II} \xrightarrow{\alpha' + \sim 180^\circ} \text{Domain III}$$

$$\text{Domain III} \xrightarrow{\chi + \sim 180^\circ} \text{Domain IV}$$

syn domain I differs from *anti* domain II in the orientation of the sugar relative to the adenine residue. An ∼180° rotation of α', which converts domain II to domain III, turns the BP long axis in the opposite direction. A ∼180° rotation in χ then produces domain IV.

Opposite Orientations are Due to Steric Hindrance Effects. To elucidate the origin of the opposite orientation effect, contour maps were prepared for each adduct by considering the van der Waals component of the total energy (Figure 8). These energy maps reveal the same overall regions below 25 kcal/mol, with the same symmetry effects as those employing the full energy potential (Figure 4). The energy boundaries above 25 kcal/mol are determined by repulsive steric components of the Lennard-Jones potential employed to compute van der Waals energies.[46] Therefore, steric repulsions are predominantly responsible for the starkly different energy landscapes in the (+)- and (−)-*trans* adducts and for the symmetries between them. Of course, the energy regions below 25 kcal/mol contain differing details in the full energy maps of Figure 4 and the van der Waals component maps of Figure 8. This stems from modulating effects due to electrostatic, torsional and other energy terms included in the total energy maps. In addition, small differences in detail stem from the nonmirror image nature of the sugars and attached C4′−C5′.

To investigate why the structures in a given domain for the (+)-*trans* adduct are disfavored for the (−)-*trans* adduct, and vice versa, we rotated each structure shown in Figure 5 into that preferred by its stereoisomer. This entailed a 180° rotation around β' in each case. The transformed structures are shown in Figures 9 and 10. Placing β' in the energetically unfavored domain for a given stereoisomeric adduct causes steric crowding between atoms on the adenine and BP residues which involve, in particular, atoms on the BP benzylic ring. In rotated Domains I and II the adenine N1 edge is in the crowded region, and in Domains III and IV the adenine N7 edge is crowded. Table 1

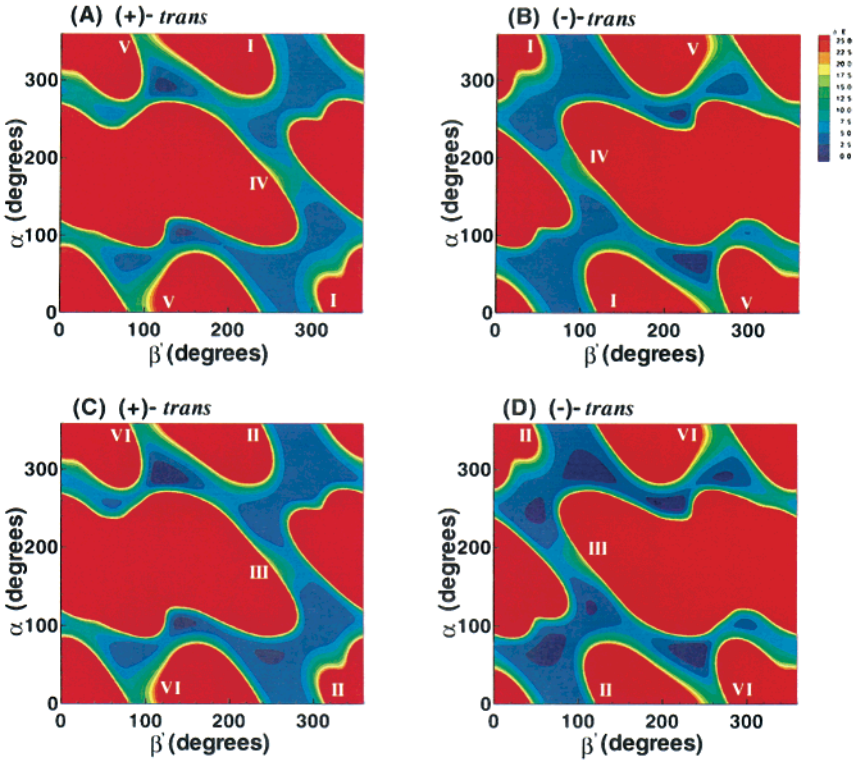

Figure 8. α', β' van der Waals energy component maps to 25 kcal/mol. I−IV denote the four low-energy domains. V and VI are higher-energy domains that do not contribute to the statistical weights. Torsion angles cycle over 360°, and thus 359° is actually contiguous with 0°: (A) (+)-*trans-anti*-[BP]−N^6-dA adduct, $\chi = 35°$ (*syn*); (B) (−)-*trans-anti*-[BP]−N^6-dA adduct, $\chi = 35°$ (*syn*); (C) (+)-*trans-anti*-[BP]−N^6-dA adduct, $\chi = 215°$ (*anti*); (D) (−)-*trans-anti*-[BP]−N^6-dA adduct, $\chi = 215°$ (*anti*).

shows the α', β' relationships among the domains. Figures 3, 4, and S3 (Supporting Information) also reveal that the low-energy domains of the (+)-*trans-anti* adduct are high energy for the (−)-*trans-anti* adduct, and vice versa, and Figure 8 pinpoints steric hindrance as the source of the opposite orientation phenomenon.

Statistical Weights and Thermodynamic Parameters. We computed the fractional statistical weights together with relative conformational free energies, enthalpies and entropies for each domain of the (+)- and (−)-*trans-anti*-[BP]−N^6-dA adduct, as described in Methods. Table 3 gives thermodynamic parameters and Table 4 gives the statistical weights. Computation of these thermodynamic parameters for each domain treats these as individual species, which is justifiable on the basis of the apparent barriers between the domains (Figures 3, 4, and S3). Differences in population and thermodynamic parameters between the (+) and the (−) adduct stem from the symmetry breaking effect of the sugar residues and C4′−C5′ atoms. It can be seen from Tables 3 and 4 that these differences are small, because the sugar is far from the adduct linkage site.

Discussion

Near-Mirror Image Symmetries, Opposite Orientations, and the Importance of the Torsion Angle β'. Our computational studies have revealed four pairs of low-energy conformational domains for the 10*S* (+)- and 10*R* (−)-*trans-anti*-[BP]N^6-dA adducts. In each domain the pyrenyl moieties adopt a mirror image symmetry as viewed along the adenine C8 containing-edge, broken, however, by the sugars and their attached C4′−C5′ groups. The energy landscapes of the two stereoisomeric adducts reveal this symmetry: they are transformable into one another by sign inversion of α' and β'. This hallmark of mirror image symmetry is rooted in the mirror image nature of substituents at the chiral carbon atoms in the BP benzylic rings in the two adducts. *Syn* domain I and *anti* domain II are most favored, with small contributions to the fractional statistical weights from *anti* domain III and *syn* domain IV. The low-energy regions of α' are at ∼0° and ∼180°, which are the same when their signs are inverted (0° = −0°; 180° = −180°). Consequently, the low-energy domains of the 10*S* (+)- and 10*R* (−)-*trans-anti* adducts actually differ from one another only by a ∼180° rotation in the torsion angle β' (Table 1). Rotation of β' from the region preferred by one stereoisomer into the β' region preferred by the other isomer causes crowding between atoms on the adenine and the benzylic ring of the BP residues. These predicted opposite orientations are completely consistent with the experimentally observed CD spectra of the stereoisomeric 10S(+)- and 10R(−)-*anti*-[BP]−N^6-dA mononucleoside adducts in solution which are near mirror images of one another.[8]

Structural Domain Preferences. α' and β' Regions. Table 1 reveals that α' is centered at 0° or 180° in each of the low-energy domains. The preference for these two α' regions stems from the maximal overlap of the adenine aromatic ring π orbitals with the N^6 lone pair p orbital when $\alpha' = \sim 0°$ or ∼180°, since the N^6 and the adenine ring p orbitals are maximally parallel in this case. With these α' values, the preferred β' are the 90° and 270°(−90°) regions. Collisions occur between the benzylic ring O9H and adenine N7 regions when α' and β' both = ∼0°, or when α' and β' both = ∼180°. Furthermore, steric clashes occur between the adenine 2−1−6 edge and the BP 11−12 edge when $\alpha' = \sim 180°$ and $\beta' = \sim 180°$, or when $\alpha' = \sim 0°$ and $\beta' = \sim 180°$.

Our results reveal that the $\alpha' = 0°$ region is favored over the 180° region in these adenine mononucleoside adducts (compare domains I and IV, and domains II and III, Table 4). In

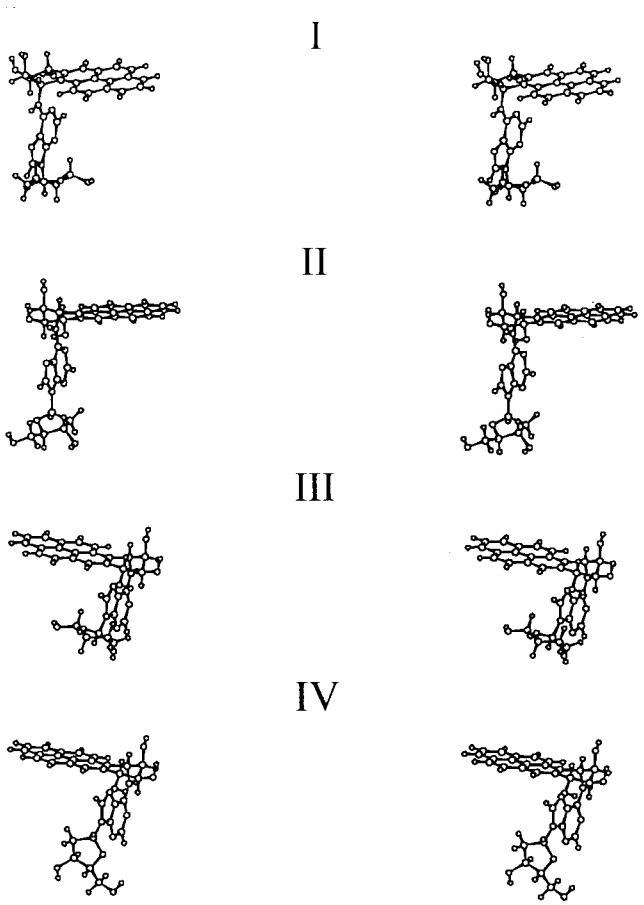

Figure 9. Stereoviews for (+) adduct structures rotated to wells of (−) adduct as detailed in Figure 5. I−IV denote four low-energy domains.

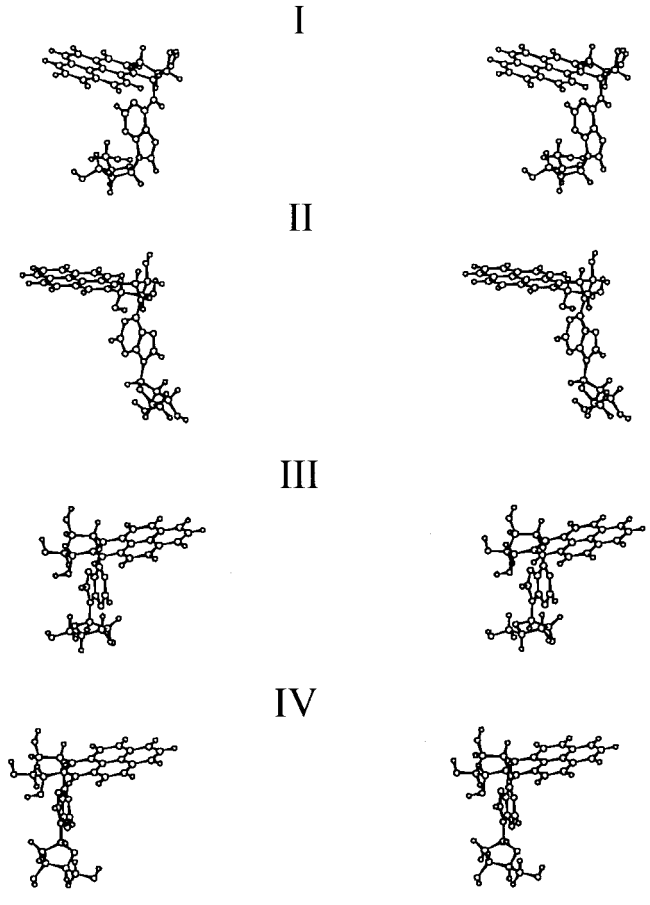

Figure 10. Stereoviews for (−) adduct structures rotated to wells of (+) adduct as detailed in Figure 5. I−IV denote four low-energy domains.

mononucleosides, the $\alpha' = 0°$ region is preferred because the adenine five-membered ring lies over the benzylic ring when α' is in the 180° region, while it is positioned further away from the benzylic ring when α' is near 0° (see Figures 6 and 7). This leads to a larger, more entropically favored $\alpha' = 0°$ region (Tables 2 and 3). However, in normal duplexes, the $\alpha' = \sim 180°$ region is required in order to form the Watson−Crick hydrogen bond that involves the free hydrogen atom on N^6-dA. Therefore, the $\alpha' = 180°$ region is more favored in duplexes.

In the 10*S* (+)- and 10*R* (−)-*trans-anti*−N^2-dG adducts, the five-membered ring of guanine is on the opposite edge of the base from the linkage site to BP, far from the benzylic ring and does not influence the preferred α' region. In the guanine adducts, the $\alpha' = 0°$ region is somewhat disfavored, because the proximity between H1(N1) and the benzylic ring causes the conformational space to be more constrained than when α' is in the 180° region.[30]

***Syn* and *anti* Conformations.** Domains I (*syn*) and II (*anti*) are essentially the same except for the difference in glycosidic torsion angles. The stabilization of domain I compared to domain II is enthalpic in origin as can be seen from the data in Table 3. The enthalpic stabilization may stem in part from a favorable electrostatic interaction that exists between the deoxyadenosine N3 and the sugar H(O5′) (N3 to H(O5′) distance = 4.49 Å); these often form a hydrogen bond when the adenine glycosidic bond adopts the *syn* orientation,[49] although they are not actually hydrogen bonded in this case. More importantly, the sugar residue is in contact with both aromatic rings of the adenine in the *syn* conformation, which contributes to the stabilization; when the adenine residue is in the *anti* orientation, the sugar contacts only its five-membered ring. This additional stabilization characteristic of the *syn* domain is therefore intrinsic to the deoxyadenosine moiety and is not significantly influenced by the BP residue.

(49) Sundaralingam, M. *The Concept of a Conformationally "Rigid" Nucleotide and its Significance in Polynucleotide Conformational Analysis*; The Israel Academy of Science and Humanities: Jerusalem, 1973; pp 417−456.

Table 3. Thermodynamics Parameters of Low-Energy Domains in 10*S* (+)- and 10*R* (−)-*trans-anti*-[BP]−N^6-dA Adducts[a]

	G (kcal/mol)		H (kcal/mol)		TS (kcal/mol)	
domain	(+)	(−)	(+)	(−)	(+)	(−)
I	−2.606	−2.605	0.788	0.794	3.394	3.399
II	−1.731	−1.649	2.628	2.699	4.359	4.349
III	0.410	0.450	4.407	4.436	3.997	3.987
IV	−0.419	−0.466	2.619	2.577	3.038	3.043

[a] *G*, *H*, and *S* are conformational free energy, enthalpy, and entropy, respectively. $T = 300$ K.

Table 4. Statistical Weights of Low-Energy Domains in 10*S* (+)- and 10*R* (−)-*trans-anti*-[BP]−N^6-dA Adducts[a]

	W%	
domain	(+)	(−)
I	79.2	81.0
II	18.3	16.3
III	0.5	0.5
IV	2.0	2.2

[a] Statistical; weights, *W*, are given in percents of the population.

Table 5. χ, α', β' Orientation in NMR Solution Structures of 10*S* (+)- and 10*R* (−)-*trans-anti*-[BP]−N^6-dA Adducts

	χ, α', β' (deg)	
duplex type	10*S* (+)	10*R* (−)
normal partner		224,141,97[a]
dG mismatch partner	21,25,270(major)[b] 242,108,178[d]	230,226,242(minor)[c]

[a] Reference 27, 224° = −136°. [b] Reference 25, 270° = −90°. [c] Reference 26, 230° = −130°, 226° = −134°, 242° = −118°. [d] Reference 28, 242° = −118°

Comparison with Preferred Conformational Domains Observed Experimentally in Stereoisomeric BP-deoxyadenosine Adducts in Solution: 3′ vs 5′ Directionality and Opposite Orientations in 10*S* and 10*R* Adducts. The sets of χ, α', β' values adopted by the 10*R* (−) and 10*S* (+)-*trans-anti*-[BP]−N6-dA adducts in double stranded DNA, determined from the analysis of high-resolution NMR data, are summarized in Table 5. We note all but one of the BP structures occur in or near the calculated low-energy α', β' regions of domains I and III shown in Figures 3−7 and Table 1. A further discussion of Table 5, giving the explanation for the anomalous α', β' domain in the NMR solution structure, of the 10R (−)-*trans-anti*-[BP]−N^6-dA adduct mismatched with dG,[28] stemming from use of an earlier AMBER force field in the NMR refinement, is provided in the Supporting Information. The *anti* domain II, preferred on the nucleoside level, is not favored relative to the *anti* domain III in duplexes because the Watson−Crick hydrogen bond involving the N^6 hydrogen atom is not possible in domain II with α' near 0°, as discussed above.

Aside from the single anomalous experimental structure, we note that all the others of Table 5 are characterized by the BP-deoxyadenosine mononucleoside adduct preferred β' values of ∼−90° for the 10*S* (+) and ∼+90° for the 10*R* (−)-*trans-anti* isomer(Table 1). This gives rise to the opposite orientations of the BP, relative to the modified deoxyadenosyl residues, observed in the duplexes containing the 10*S* (+)- and 10*R* (−)-*trans-anti*-[BP]−N^6-dA adducts. Thus, the β' domain governs the opposite orientation phenomenon in the 10*R* and 10*S* adducts that are derived from the (−)- and (+)-*anti*-BPDE enantiomers, respectively. In the observed domains I and III, the BP moiety is placed on the 3′-side of the modified adenine in the 10*S* (+)-*trans-anti* adduct, and on the 5′-side in the 10*R* (−)-*trans-anti*-isomeric adduct (see Figures 2, 6, and 7).

By contrast, however, our computed domains II and IV which have not yet been observed, place the BP on the 5′-side of the modified dA residue in the 10*S* isomer, and on the 3′-side in the 10*R* isomer. The key point is the opposite orientations in a given domain adopted by the 10*S*/10*R* pair, which is determined by the favored β' region, rather than the 3′- or 5′-direction. Domains II and IV could be particularly relevant where Watson−Crick pairing is not possible, such as in single strands or with a mismatched base opposite the modification site; then domain II with $\alpha' = 0°$ or domain IV with χ in the abnormal *syn* region could become more favored.

Another subtle point, which can be discerned from Figure 5, is that it is possible for a (+) stereoisomer to adopt one domain and a (−) stereoisomer to adopt another (domains I and IV, or II and III), such that the BP moiety is pointing in the same direction relative to the 3′- or 5′-sugar direction in both isomers, while β' remains in its preferred region in each case.

The more difficult way for the BP residues in a 10*S*/10*R* pair to have the same orientation would entail adopting the wrong β' domain for that isomer. The energy maps of Figure 4 reveal higher-energy wells at ∼9−12 kcal/mol at β' ∼90° (domains V and VI) for the 10*S* (+) adduct and at β' ∼−90° for the 10*R* (−) adduct. These correspond to structures where the BP orientations and corresponding β' values of one stereoisomer are rotated to the domain I or II favored by the other isomer, i.e. the wrong β' domain, as shown in Figures 9 and 10. While these higher-energy wells have no fractional statistical weights, a ∼9−12 kcal/mol energy difference might be surmountable in a biological context, perhaps allowing for some structures with the BP residue oriented in directions opposite to those preferred, via adoption of the wrong β' domain. However, this possibility appears to be less in the 10*S* (+)- and 10*R* (−)-*trans-anti*-[BP]−N^6-dA adducts than in the corresponding N^2-dG adducts,[30] since a small but nonzero statistical weight was computed for the wrong β' domain in these adducts.

It is remarkable that opposite orientations of the aromatic BP ring system relative to the plane of the modified adenine residue are maintained in the NMR solution structures of the DNA duplexes (Table 5) despite the asymmetric nature of the double stranded DNA resulting from the 5′ → 3′ strand polarity. This opposite orientation phenomenon stems from the primary steric hindrance effects between atoms on the modified adenine and the covalently attached BP residue.[29] These opposite orientations have a profound influence on the thermodynamic melting temperatures (T_m) of the duplexes containing the stereoisomeric 10*S*(+)-*trans-anti* and the 10*R*(−)-*trans-anti*-[BP]−N^6-dA adducts reported by Schurter et al.[28] The duplex with the 10*S*(+)-*trans* adduct exhibits a lower T_m than the duplex with the isomeric 10*R*(−)-*trans* adduct, suggesting that the former adduct is in a less stable and structurally more distorted conformation. These differences, which may elicit different biochemical or biological responses,[29] are clearly a result of the opposite orientations of the BP ring systems relative to the modified adenine residues in DNA, stemming from steric hindrance effects at the [BP]-dA adduct level (Figures 6 and 7). In turn, the DNA strand polarity of the double helix results in differences in the interactions between the bulky aromatic ring of the BP residues with neighboring nucleotide residues, on the 5′- or 3′-side of the modified base, as discussed by Schwartz et al.[26] In the 10*S* adduct, the aromatic ring may give rise to steric crowding with residues on the 5′-side of the modified dA residue, thus destabilizing the duplex and leading to a lower T_m; in the case of the 10*R* adduct, there appears to be less crowding between the aromatic ring of the BP and the residues on the 3′-side of the modified dA (Figure 2). The slightly greater preference for the *syn* orientation of the glycosidic linkage in 10*S* adducts (Table 5) also results from the fact that the 10*S* and 10*R* adducts intercalate to opposite sides of the asymmetric DNA duplex, with attendant symmetry-breaking differences in local interactions between the BP and DNA bases and phosphodiester-sugar backbone. Again, this is a consequence of the primary steric hindrance effect at the [BP] residue-adenine mononucleotide adduct level that manifests itself in double stranded DNA.

Comparisons of Conformational Domains Preferred by 10*S* (+)- and 10*R* (−)-*trans-anti*-[BP]−N^2-dG Adducts. Our earlier study of the 10*S* (+)- and 10*R* (−)-*trans-anti*-[BP]−N^2-dG adducts on the nucleoside level also revealed four low-energy domains for each isomer.[30] Domains I, II, and III are quite similar in guanine and adenine adducts(Table 1) with the same absolute configuration at C10, while domain IV differs in both χ and β'. However, the relative statistical weights differ markedly. Domain I is strongly preferred in the adenine adduct with domain II next in preference, while in guanine adducts

domain III is the most favored, followed by II. In guanine adducts, the BP moiety is linked at the N^2 position, which is much closer to the sugar than in adenine adducts, in which BP is linked to N^6 − on the edge of adenine that is opposite to the sugar. When the glycosidic torsion angle is *syn*, the sugar is closer to N^2 than when it is *anti*. The presence of a BP moiety on guanine N^2 makes the *syn* region even more crowded and hence less favored than when the BP is linked to N^6 of adenine. This accounts for the much lower preference of domain I in the guanine adducts. In addition, as discussed above, the guanine adducts favor the $\alpha' = 180°$ region more than the adenine adducts because of the differing position of the purine five-membered ring in relation to the benzylic ring in the adenine versus guanine adducts.

Classical Intercalation in 10*S* (+)- and 10*R* (−)-*trans-anti*-[BP]−N^6-dA Adducts and Minor Groove Positions in N^2-dG Adducts. While the 10*S* (+)- and 10*R* (−)-*trans-anti*-[BP]−N^6-dA adducts are intercalated into the helix without displacement of the modified adenine bases, the analogous N^2-guanine adducts are positioned in the minor groove of a normal B-DNA duplex[17−19] (or in a base displaced intercalated position in a duplex in which the modified base has no partner base[21,24a]). The advantage of classical intercalation, seen most clearly in the structure of the 10*R* (−)-*trans-anti*−N^6-dA adduct with a normal partner base thymine[27] (Figure 2 C), is in the insertion of the hydrophobic BP into the helix. In this intercalated, base-stacked conformation, the interaction of the hydrophobic BP residue with the aqueous solvent is minimized with attendant favorable BP-base stacking interactions, and the hydrophilic benzylic ring and its hydroxyl groups are exposed to the solvent and protrude into the major groove. While these effects are energetically favorable, the associated effects of stretching and unwinding the helix to create the intercalation pocket, as well as some distortion (though not complete rupture) of the base pairing at the lesion site, are energetically unfavorable. The energetically favorable aspects of minor groove N^2-dG adduct conformations are (1) maintenance of nearly normal Watson−Crick base pairing and stacking, (2) one face of the hydrophobic pyrenyl ring system positioned in the minor groove is shielded from the aqueous solvent, and (3) the hydrophilic benzylic ring hydroxyls are exposed to solvent. An unfavorable aspect is the exposure of one face of the aromatic pyrenyl ring system to the aqueous solvent environment. In addition, it appears that classical intercalation of the covalently linked BP moiety would be more difficult from the narrow minor groove side as it requires insertion of the BP moiety without displacement of the modified base. In the case of the [BP]−*N*^{2}-dG adducts the energetic advantages of the minor groove position dominate.

Since the N^6-dA adduct is positioned on the major groove side in a normal B-DNA double helix, there is a possibility that the BP residue could be positioned in the major groove, with full maintenance of Watson−Crick hydrogen bonding. However, since the major groove is rather spacious, bulky aromatic carcinogens positioned in the major groove, observed in the case of 2-aminofluorene(AF) bound to guanine C8, can be exposed to the aqueous solvent on both faces.[50−53] Solvent exposure on both sides of the hydrophobic BP four-ring aromatic residue positioned in the major groove would be unfavorable and could exceed the cost of intercalation. Figure 11 shows an energy minimized major groove conformer for the 10*S* (+)-*trans-anti*-[BP]−N^6-dA adduct, obtained as described in the Methods section. This structure reveals the large solvent exposed area of the hydrophobic pyrenyl ring system. χ, α', β' values in this structure are 221.3°, 2.1°, 343.0° respectively. We estimated the hydrophobic free energy cost of retaining the aromatic pyrenyl ring system of the BP moiety in the aqueous solvent in this major groove structure by computing the solvent-exposed area of the aromatic pyrenyl ring system. We obtained a contact area of 69.7 Å^2. Using the relationship described in Methods, we compute the cost of cavity formation in aqueous solvent by the hydrophobic pyrene, i.e. the cost of the entropic hydrophobic effect, and obtain an energy penalty of 3.3 kcal·mol^{-1} (Enthalpic van der Waals interactions between the BP and water, when the BP is in the major groove, are taken to be approximately equivalent to van der Waals interactions between the BP and DNA when the BP is intercalated). By comparison, the entropic hydrophobic energy penalty for the single aromatic ring in the (S)-α−N^6-dA styrene oxide adduct, positioned in the major groove in the NMR solution structure,[37] provides a solvent exposed area of 28.7 Å^2 and a calculated cost for the entropic hydrophobic effect of only 1.4 kcal/mol.

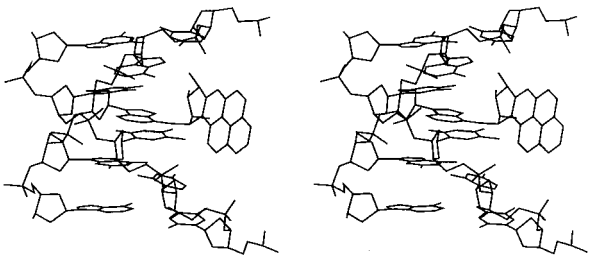

Figure 11. Stereoview of energy minimized (+)-*trans-anti*-[BP]−N^6-dA adduct in B-DNA major groove. Central 5-mer of duplex 11-mer is shown.

Conclusions

The opposite orientations of the BP moiety observed in solution structures of 10*S* (+)- and 10*R* (−)-*trans-anti*-[BP]−N^6-dA adducts in duplex DNA, namely 3′- or 5′-directed classical intercalation without displacement of the modified base,[25−28] stems from steric hindrance originating in the mirror image nature of the benzylic ring in the stereoisomeric adduct pair, which governs the conformations even on the nucleoside level. Since the opposite orientation phenomenon is essentially steric in origin, and intrinsic to the stereochemical nature of the covalent linkage, it may well persist in a biological context and influence treatment of the lesions by cellular enzymes, although a subtle possibility for adoption of similar orientations by a 10*S*/10*R* isomer pair, especially in single strands or mismatched duplexes, without violating steric hindrance, was noted. Differential rates, or efficiencies of DNA synthesis catalyzed by polymerases during in vivo and in vitro replication studies past the lesions have, in fact, been observed.[13] In addition, in vitro exonuclease digestion studies[54] have revealed differential processing of the two lesions. Furthermore, differential treatment of the two lesions by T7 RNA polymerase in terms of degree of bypass and mutagenic transcription has also been reported.[55] The [BP]−N^6-dA adducts adopt non-base displaced, intercalated orientations rather than major groove positions in order to minimize aqueous solvent exposure of the large hydrophobic pyrene ring system. Thus, very fundamental

(50) Eckel, L. M.; Krugh, T. R. *Nat. Struct. Biol.* **1994**, *1*, 89−94.
(51) Eckel, L. M.; Krugh, T. R. *Biochemistry* **1994**, *33*, 13611−24.
(52) Mao, B.; Hingerty, B. E.; Broyde, S.; Patel, D. J. *Biochemistry* **1998**, *37*, 95−106.
(53) Patel, D. J.; Mao, B.; Gu, Z.; Hingerty, B. E.; Gorin, A.; Basu, A. K.; Broyde, S. *Chem. Res. Toxicol.* **1998**, *11*, 394−407.
(54) Chary, P.; Lloyd, R. S. *Chem. Res. Toxicol.* **1996**, *9*, 409−17.
(55) Remington, K. M.; Bennett, S. E.; Harris, C. M.; Harris, T. M.; Bebenek, K. *J. Biol. Chem.* **1998**, *273*, 13170−6.

chemical forces, steric and hydrophobic, in stereoisomeric 10*S* (+)- and 10*R* (−)-*trans*-*anti*-[BP]−N^6-dA adducts govern the conformations and biological functioning of these adducts.

Acknowledgment. This research is supported by NIH Grants CA 28038 and RR-06458, and DOE Grant DE-FG0290ER60931 to S.B., and NIH Grant CA-20851 to N.E.G. We thank Professor Robert Shapiro, New York University, for insightful discussions and Professor Robert Topper, The Copper Union, and Professor Wilma Olson, Rutgers University, for helpful advice.

Supporting Information Available: A further discussion of Table 5 is provided. In addition, three tables are given. Table S1 lists conformational features of energy-minimized modified bases in the starting structures. Table S2 gives additional force field parameters. Table S3 gives partial charges, topology, and atom type assignments for the 10*S* (+)- and 10*R* (−)-*trans*-*anti*-[BP]−N^6-dA nucleoside adducts and the respective base-only adducts. Three figures are also provided. Figures S1 and S2 show the full set of α',β' energy contour maps at 5° intervals of χ for the 10*S* (+)- and 10*R* (−)-*trans*-*anti*-[BP]−N^6-dA adducts, respectively. Figure S3 shows van der Waals component energy maps for each adduct (PDF). This material is available free of charge via the Internet at http://pubs.acs.org.

JA993624H